3-D MHD SIMULATIONS OF THE SOLAR CONVECTION ZONE AND TACHOCLINE

Allan Sacha Brun

DSM/DAPNIA/Service d'Astrophysique, CEA-Saclay, 91191 Gif-sur-Yvette Cedex, France.

ABSTRACT

We present the recent progress made in modelling in three dimensions, with the anelastic spherical harmonic (ASH) code, the solar convective envelope and the tachocline at its base. We discuss our current understanding of the physical processes thought to be at the origin of the solar differential rotation and meridional circulation, how they interact and what are the implications for the working of the solar dynamo. We show that the tachocline must play a crucial role in the generation and amplification of the global and ordered solar magnetic fields since the turbulent convection zone produces mostly non-axisymmetric ($m \neq 0$) magnetic fields. Given the central role played by the tachocline in the solar cycle, we present undergoing numerical efforts to understand its dynamics and its thinness (e.g. $\leq 0.05 R_\odot$) and comment upon the coupling between the solar radiative interior and its convective envelope. Finally we propose possible future routes toward a fully self-consistent three dimensional model of the Sun.

Key words: sun: convection, rotation, magnetism.

1. INTRODUCTION

The Sun is a magnetically active star, possessing a wide range of dynamical processes (see for instance Stix 2002). Most striking is that the Sun exhibits a pronounced differential rotation in latitude and radius and 22-year cycles of global magnetic activity, involving sunspot eruptions with very well defined rules for field parity and emergence latitudes as the cycle evolves. Coexisting with these large-scale ordered magnetic structures are small-scale but intense magnetic fluctuations that emerge over much of the solar surface, with little regard for the solar cycle. These phenomena have been revealed with astonishing details by observations made with the latest instruments on the ground (Gong+, 1-m Swedish Solar Telescope) and onboard satellites (Trace, SoHO). Understanding those phenomena and observations require state-of-the art numerical simulations supported by theoretical models. The complex and nonlinear magnetic phenomena present in the Sun are thought to be linked to the presence of a dynamo in its interior, resulting from the subtle interaction between turbulent convection, rotation, shear and magnetic fields. Since the magnetic fields, like the underlying turbulence, can be both orderly on some scales and chaotic on others, this diverse range of activity is most likely generated by two conceptually distinct magnetic dynamos (e.g., Weiss 1994; Cattaneo & Hughes 2001; Ossendrijver 2003): a *small-scale dynamo*, functioning within the intense turbulence of the upper convection zone, that builds the chaotic magnetic fluctuations, and a *global dynamo*, operating both within the deeper convection zone and the strong rotational shear of the tachocline at its base, that builds the more ordered fields. Given the wide range of temporal and spatial scales coexisting in the physical processes at work in the Sun, it is a great challenge, even for today's supercomputers, to model self-consistently the solar interior and dynamo. However, it is possible to split the solar dynamo problem into several 'blocks' that could answer specific points of this complex problem. We have followed such an approach by studying with the ASH code some key ingredients of the solar dynamo, such as the establishment of the solar differential rotation profile by turbulent convection, the characteristics of the mean and fluctuating dynamo induced magnetic fields via shear (e.g, ω-effect), helical convection (e.g, α-effect) or non axisymmetric dynamo effects. More recently we have also started studying the dynamics of the solar tachocline. We would like here to summarize our findings and discuss the challenges that remain to be addressed in the forthcoming future.

2. THE ANELASTIC SPHERICAL HARMONIC CODE

In this study we use the ASH code (Clune et al. 1999, Miesch et al. 2000, Brun et al. 2004) to model the solar interior. The ASH code solves the full set

of 3–D MHD anelastic equations of motion in a rotating spherical shell (with or without convection) with high resolution on massively-parallel computing architectures. These equations are fully nonlinear in velocity and magnetic field variables, but under the anelastic approximation the thermodynamic variables are linearized with respect to a spherically symmetric and evolving mean state.

The velocity, magnetic, and thermodynamic variables are expanded in spherical harmonics $Y_{\ell m}(\theta, \phi)$ for their horizontal structure and in Chebyshev polynomials $T_n(r)$ for their radial structure. This approach has the advantage that the spatial resolution is uniform everywhere on a sphere when a complete set of spherical harmonics is used up to some maximum in degree ℓ (retaining all azimuthal orders $m \leq \ell$ in what is known as triangular truncation).

The anelastic approximation captures the effects of density stratification without having to resolve sound waves which would severely limit the time step. In the MHD context, the anelastic approximation filters out fast magneto-acoustic waves but retains the Alfven and slow magneto-acoustic modes. In order to ensure that the mass flux and the magnetic field remain divergenceless to machine precision throughout the simulation, we use a toroidal–poloidal decomposition. Contact is made with a realistic solar interior by using for the initial mean structure an accurate 1–D solar model (Brun et al. 2002).

3. CHALLENGES IN MODELLING THE SOLAR CONVECTION ZONE

The solar convective envelope is highly turbulent with corresponding large values of both the Reynolds and magnetic Reynolds numbers $Re = vL/\nu$ et $Rm = vL/\eta$ (greater than 10^8, where v, L, ν and η are respectively a representative convective velocity, length and the viscous and magnetic diffusivities). Constructing accurate numerical models of such a turbulent and complex dynamical system is difficult, numerically stiff, and require powerful computers. An extensive litterature has been devoted to this problem and can be mainly separated into two numerical approaches: highly turbulent but local models in cartesian geometry (Brandenburg & et al. 1996, Brummell et al. 1998, Stein & Nordlund 2000, Cattaneo & Hughes 2001, Robinson & Chan 2001, Tobias et al. 2001) or mildly turbulent but global-scale models in spherical geometry (Glatzmaier & Gilman 1982, Gilman 1983, Glatzmaier 1987, Miesch et al. 2000, Brun et al. 2002, 2004). The progress made with parallel computers over the past 20 years has allowed to improve the physical content of the numerical simulations which now make reasonnable contacts with helioseismic inversions and surface observations of the Sun. However major challenges remain to understand fully its turbulent convection, internal rotation profile and magnetic activity.

3.1. Model Description

Our model is a simplified description of the solar convection zone: solar values are taken for the heat flux, rotation rate, mass and radius, and a perfect gas is assumed. The computational domain extends from 0.72 to 0.97 R (with R the solar radius), thereby concentrating on the bulk of the unstable zone and here not dealing with penetration into the radiative interior nor with the partially ionized surface layers. The typical density difference across the shell in radius is about 30. The grid resolution used in this MHD simulation is $N_r \times N_\theta \times N_\phi = 128 \times 512 \times 1024$ (higher resolution has been achieved in purely hydrodynamical simulations, Brun et al. 2005). In the case considered here, namely *M3*, the simulation possesses Prandtl and magnetic Prandtl numbers of respectively $Pr = \nu/\kappa = 1/8$ and $Pm = \nu/\eta = 4$. The rms Reynolds and magnetic Reynolds numbers, evaluated with effective turbulent value for ν and η are typically $Re = 110$ and $Rm = 500$ (see Brun et al. 2004 for more details).

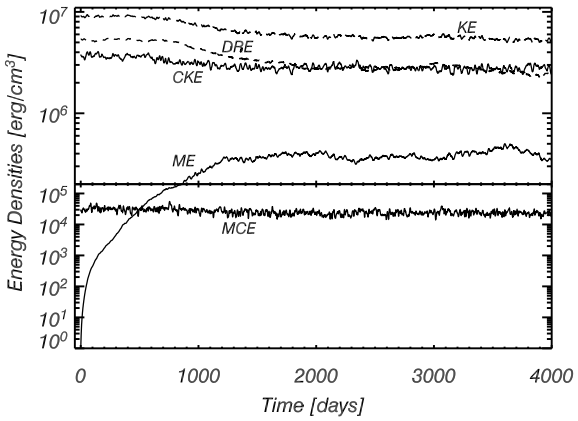

Figure 1. Kinetic (KE) and magnetic energy (ME) time traces for case M3. Also shown are the kinetic energies contained in meridional flows (MCE), differential rotation (DRE) and non axisymmetric convective motions (CKE). Note the significant decrease of DRE as ME grows and becomes larger than MCE.

The effects of the steep entropy gradient close to the surface has been softened by introducing a subgrid scale (SGS) transport of heat to account for the unresolved motions, and enhanced diffusivities are used in these large eddy simulations (LES). The boundary conditions at the top and bottom of the computational domain are stress-free impenetrable walls for the velocity field, constant entropy gradient for the entropy and match to a potential field for the magnetic field.

We start our MHD simulations from an already evolved and equilibrated purely hydrodynamical so-

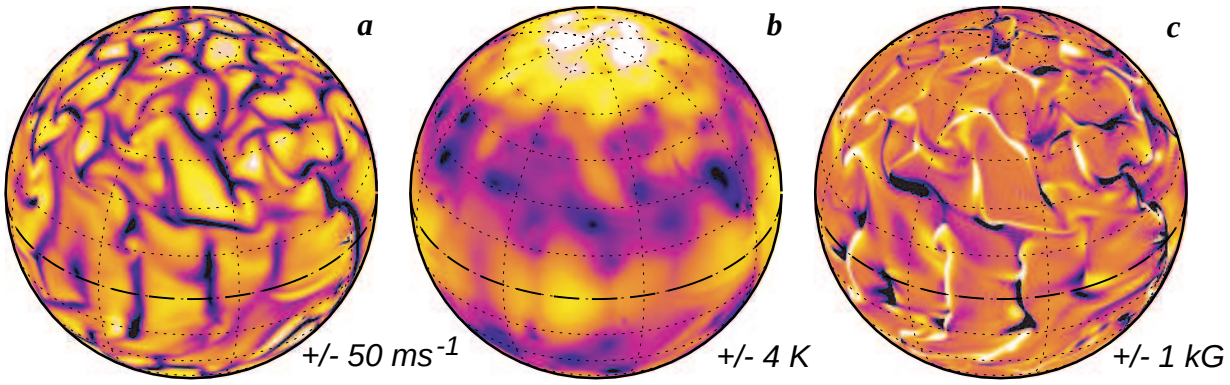

Figure 2. Snapshot of the radial velocity (a), temperature (b) and radial magnetic field (c) near the top of the domain for case M3. Typical field strengths are indicated, with dark tones corresponding to downward velocities and negative temperature fluctuations and polarities. The dashed line indicates the equator.

lution, namely case H, that possesses a strong almost solar-like differential rotation (see left panel of Figure 5). A seed axisymmetric dipolar magnetic field is then introduced in the convective spherical shell and the simulations evolved in time.

3.2. Convection and Dynamo Action

Figure 1 shows the kinetic and magnetic energy time traces over 4000 days of simulated time of case *M3*. We see that the magnetic energy (ME) grows by many order of magnitude through dynamo action. After 1200 days, the ME saturates, due to the nonlinear feed back of the Lorentz forces, to a value of about 7% of the KE and retains that level for more than 3 ohmic decay times. Upon saturation, the kinetic energy (KE) in the model has been reduced by about 40% compared to its initial value, say KE_0, given by case H. This change is mostly due to a reduction of the energy contained in the differential rotation (DRKE) which drops by over 50%. By contrast, the energy contained in the convective motions (CKE) only decreases by about 27%, which implies an increased contribution of the non-axisymmetric motions to the total kinetic energy balance. For case *M3*, the decrease in KE first becomes apparent after about 600 days of evolution, when the ME reaches roughly 0.5% of KE_0, attaining a value larger than that contained in the meridional circulation kinetic energy (MCE).

The total kinetic and magnetic energies are small compared to the total potential, internal and rotational energies contained in the shell. The magnetic energy must arise from the conversion of kinetic energy but this does not necessarily lead to a decrease in the total kinetic energy because the motions may draw upon the other reservoirs. Yet, in all of our magnetic simulations, energy is redistributed such that the sum of the kinetic and magnetic energy is less than the total kinetic energy KE_0 contained in case H. The net energy deficit can be attributed primarily to the reduction in strength of the differential rotation by Maxwell stresses. This means that in a convection zone the way the energy is redistributed among and within the different reservoirs is modified by the presence of magnetic field, but these modifications remain moderate in the case presented here. In addition our choice of magnetic boundary conditions (potential field) could explain for some part the decrease of KE+ME since it correspond to a net Poynting flux at the boundaries.

A detailed analysis of the redistribution of ME within its mean and fluctuating components reveals that the magnetic energy contained in the mean-field components ($m = 0$) represents only 2% of total ME with the 98% remaining contained in the non-axisymmetric fluctuations. Most of the mean-field energy is in the toroidal field (1.5%), which exceeds the energy in the poloidal field by about a factor of three due to the stretching and amplification of toroidal field by differential rotation (the ω-effect). This ratio is smaller than in the Sun, where the mean toroidal field is estimated to be about two orders of magnitude more energetic than the mean poloidal field. This discrepancy can again be attributed to the absence of an overshoot region and a tachocline, where toroidal field can be stored for extended periods while it is amplified by relatively large angular velocity gradients (see §4). For the non-axisymmetric fluctuations, the magnetic energy is approximately equally distributed among the toroidal and poloidal fields, indicating that the turbulent convection can efficiently generate both components in roughly equal measure, implying that the ω-effect plays a lesser role. The radial profile of ME peaks at the bottom of the domain, due to the downward transport of magnetic fields by turbulent plumes. Magnetic fields generation through dynamo action is present at all scales, with ME being in superequipartition over degree $\ell \sim 20$.

In order to illustrate the complex interplay between

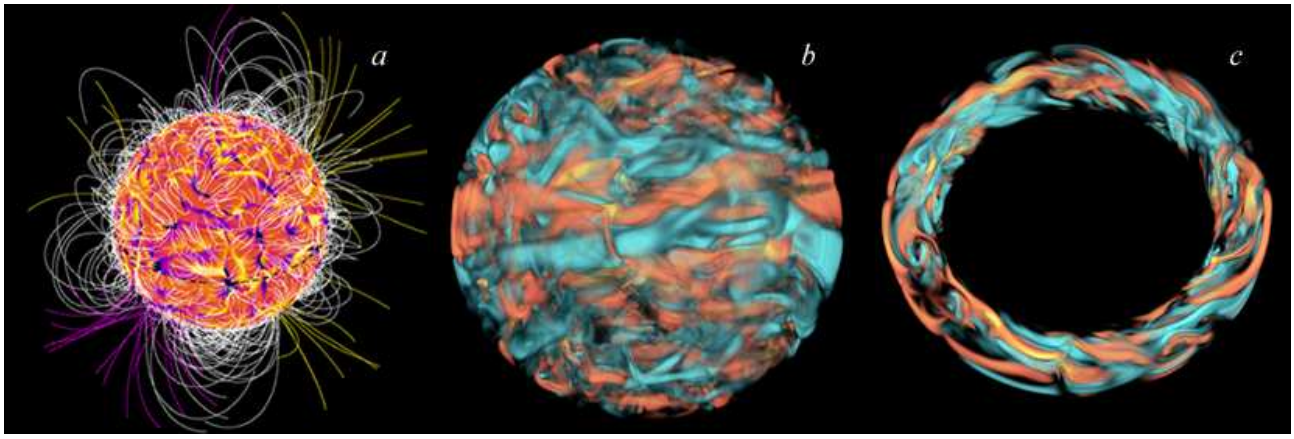

Figure 3. (a) Potential extrapolation of the magnetic field, with closed magnetic loops in white, and respectively outward (inward) open fields lines in yellow (magneta). As background image, the radial component of magnetic field at the top of the domain serves as starting point for the foot lines. (b) Full sphere rendering of the toroidal magnetic field with blue (red) tones corresponding to negative (positive) polarity. (c) close up view on the equatorial region revealing the entangled and intertwined nature of the toroidal field due to the combined action of the α and ω-effect.

convective motions, differential rotation and magnetic fields, we display the structure of the convection and magnetic fileds of *M3* in Figures 2 and 3. The convective patterns are qualitatively similar to the hydrodynamic progenitor case H. The radial velocity (Fig. 2a) is dominated by narrow cool downflow lanes and broad warm upflows, with a more isotropic behavior at higher latitudes. The charactristic spatial scale here is larger than supergranulation, which is as of today, the smallest convective scale that such global models can simulate but in rather thin shell (see Derosa, Gilman & Toomre 2002). The temperature fluctuations (Fig. 2b) exhibit a banded appearance most likely linked to an inner thermal wind, that contributes somewhat to the establishment of the differential rotation (see §3.3). The much smoother appearance of the temperature fields is due to our choice of a small Prandtl number (Pr=1/8). We can see that the strongest vortices correlated well with the coldest fluctuations resulting in an outward transport of heat.

The radial magnetic field (Fig. 2c) is found to be concentrated in the downflow lanes, with both polarities coexisting having beed swept there by the horizontal diverging motions at the top of the domain. The Lorentz forces in such localized regions have a noticable dynamical effect on the flow, with ME sometimes being locally bigger than KE, influencing the evolution of the strong downflow lanes via magnetic tension that inhibits vorticity generation and reduces the shear. The magnetic field generally has a finer and more intricate structure than the velocity field due to the smaller diffusion ($P_m = 4$ in this simulation) and also due to the nature of the advection terms in the induction equation, which are similar in form to those in the vorticity equation (e.g. Biskamp 1993). The magnetic field and the radial velocity

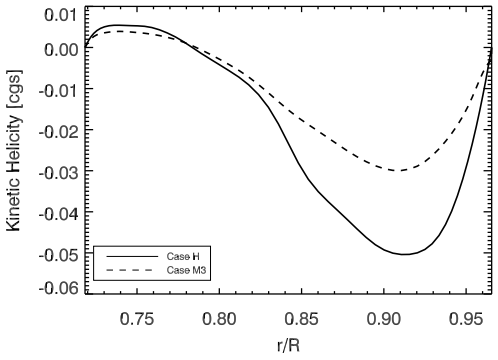

Figure 4. Radial profile of the kinetic helicity in cases H and M3. The presence of magnetic fields lead to a reduction of the amplitude of the kinetic helicity.

possess a high level intermittency both in time and space, revealed by extended wings in their probality distribution functions and are quite asymmetric (Brun et al. 2004). The longitudinal velocity v_ϕ is much more gaussian-like. These results are in good agreement with simulations of compressible MHD turbulence in cartesian geometry (Brandenburg et al. 1996).

In Figure 3a we represent the potential extrapolation of the radial magnetic field at the top of the computational domain. We see that the field can take the form of magnetic loops connecting either local or widely separated areas as well as be open, with respectively outward (inward) field lines in yellow (magenta). The longitudinal magnetic field is shown in the companion Figures 3b and 3c using respectively a global view of the domain or a zoomed

in view around the equator to reveal its ribbon-like structures. The toroidal field B_ϕ near the surface appears more distributed and more patchy than B_r, characterized by relatively broad regions of uniform polarity, particularly near the equator (Fig. 3c). The magnetic field topology generally does not exhibit any clear symmetries about the equator, although some of the B_ϕ elongated features at low latitudes do have an antisymmetric counterpart.

The rigidifying effect of the magnetic fields on the convective motions, mainly in location of strong vorticity and shear, is clearly evident in Figure 4 where we show a plot of the radial profile of the kinetic helicity $H_k = \mathbf{v} \cdot \omega$ for both case H and *M3*. We can see that case *M3* possesses a smaller kinetic helicity throughout the domain, with minimum and maximum peak reduced by about 30%. However H_k retains the same sign at the top (negative) and bottom (positive) of the shell in both cases.

3.3. Differential Rotation

Helioseismic inversions of large-scale, axisymmetric, time-averaged flows in the Sun currently provide the most important observational constraints on global-scale models of solar convection. Such flows (averaged over longitude and time) have therefore been a primary focus of previous simulations of the solar convection zone (Glatzmaier 1987; Miesch et al. 2000; Brun & Toomre 2002). Of particular importance and reasonnably well constrained by helioseismology, is the mean longitudinal flow, i.e. the differential rotation $\Omega(r, \theta)$, which is characterized by a fast equator, slow poles and a profile almost independant of radius at mid latitudes (Thompson et al. 2003).

In Figure 5 (left panel), we display the time-averaged angular velocity profile achieved in the purely hydrodynamic case H. This case possesses a fast equator, a monotonic decrease of Ω with latitude and some constancy along radial line at mid latitudes, all these attributes being in reasonnable agreement with helioseismic inferences. With fairly strong magnetic fields sustained within the bulk of the convection zone in case *M3*, it is to be expected that the differential rotation Ω established in the progenitor case H will respond to the feedback from the Lorentz forces. Figure 5 (middle panel) shows the time-averaged angular velocity achieved in case *M3*, which exhibits a prograde equatorial rotation with a monotonic decrease in angular velocity toward higher latitudes as in the Sun. The main effect of the Lorentz forces is to extract energy from the differential rotation. The kinetic energy contained in the differential rotation drops by a factor of two after the addition of magnetic fields and this decrease accounts for over 70% of the total kinetic energy difference found between the two cases (see §3.2). This is reflected by a 30% decrease in the angular velocity contrast $\Delta\Omega$ between the equator and latitudes of 60°, going from 140 nHz (or 34% compared to the reference frame Ω_o) in the hydrodynamic case H to 100 nHz (or 24%) in case *M3*. This value is close to the contrast of 22% inferred from helioseismic inversion of the solar profile (Thompson et al. 2003). Thus the convection is still able to maintain an almost solar-like angular velocity contrast despite the inhibiting influence of Lorentz forces.

A careful study of the redistribution of the angular momentum in our shell reveals that the source of the reduction of the latitudinal contrast of Ω can be attributed to the poleward transport of angular momentum by the Maxwell stresses (cf. Brun 2004, Brun et al. 2004). The large-scale magnetic torques are found to be 2 orders of magnitude smaller, confirming the small dynamical role played by the mean fields in our MHD simulation. The Reynolds stresses now need to balance the angular momentum transport by the meridional circulation, the viscous diffusion and the Maxwell stresses. This results to a less efficient speeding up of the equatorial regions. Since ME in case *M3* is only 7% of KE, the Maxwell stresses are not yet the main players in redistributing the angular momentum and case $M3$ is able to sustain a strong differential rotation as observed in the present Sun. At higher level of magnetism with ME near equipartition with KE, the differential rotation is severely damped and no more solar-like. The somewhat faster rotation rate and larger $\Delta\Omega$ in case H relative to case *M3* further suggests that a reduced level of the Sun's magnetism (as during the Maunder minimum) may lead to greater differential rotation. Some evidence seem to confirm it (Eddy et al. 1976, Brun 2004).

There is actually some debates on the relative importance of the thermal wind linked to baroclinic effects compared to the Reynolds stresses in establishing the solar differential rotation. Several authors (Rudiger & Kitchatinov 1995, Robinson these proceedings, Durney 1999) advocate that the thermal wind (cf. Pedlosky 1987, Brun & Toomre 2002) dominates the delicate balance that leads to the observed angular velocity profile. In our 3–D simulations we do find that the thermal wind account for a fraction of the differential rotation profile in the bulk of the convection zone, but there are many locations, mainly close to high shearing regions, where it does not. At the onset of the convection instability in the simulation, it is difficult to say if it is the turbulent convective motions that transport angular momentum via Reynolds stresses to establish a differential rotation that imprint itself in the thermodynamics variables, or if the convection via anisotropic latitudinal transport of heat, estalished the entropy and temperature contrasts that lead to a stong thermal wind that established the differential rotation. Certainly both effects contribute to Ω, but in a turbulent flow such as the solar convection zone, the Reynolds

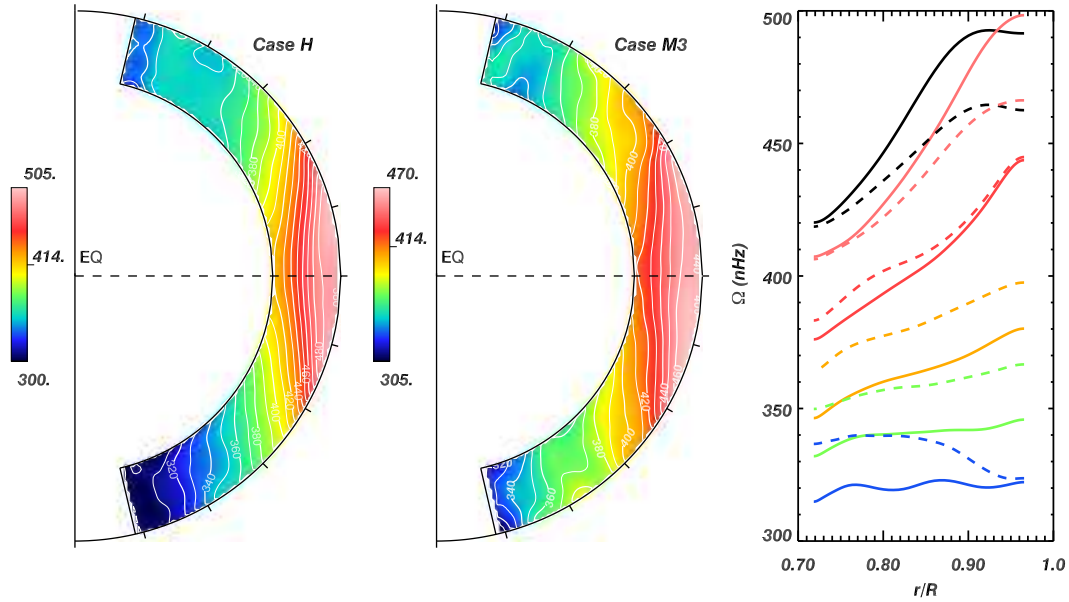

Figure 5. Temporal and longitudinal averages of the angular velocity profiles (converted to nHz) achieved in case H and M3 over an interval of 100 days (shown as contour plots). These cases exhibit a prograde equatorial rotation and a strong contrast $\Delta\Omega$ from equator to pole, as well as possess a high latitude region of particularly slow rotation. In the right panel, displaying radial cuts of Ω (with the equatorial cut on top and decreasing latitudes as we go down) for both cases, the reduction in $\Delta\Omega$ due to the nonlinear feed back of the Lorentz forces (solid vs dashed lines) can be assessed

stresses must be important players and indeed we do find in our simulations that there are the only agent transporting the angular momentum equatorward.

3.4. Meridional Circulation and the Solar Cycle

The meridional circulation plays an important role in mean field models of the solar dynamo, particularly in models of the Babcock-Leighton type also called flux transport models (Dikpati & Charbonneau 1999; Dikpati this proceedings). Inferring its radial and latitudinal profile in the Sun would help greatly our understanding of the solar dynamo and its 22-year cycle. Several technics such as dopler mesurement, time distance and ring diagram analysis (see Haber et al. these proceedings for details) have been used to probe the meridional circulation established in the Sun. These methods are reliable only in the upper parts of the surface layers (say $r > 0.95R$) and reveal one big cells in latitude, except during solar maximum where the northern hemisphere exhibits two cells (see Haber et al. 2002). Deeper down ($r \sim 0.85$ being the deepest as of today) the inferences become somewhat more uncertain. Our simulation of turbulent convection are helpful in improving our physical intuition on the processes establishing this weak flow and its mean profile.

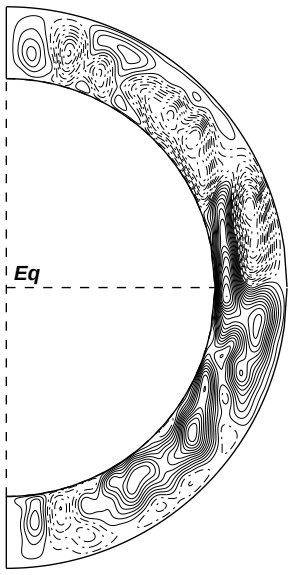

Figure 6. Temporal and longitudinal average of the meridional circulation realized in case M3 (shown in a meridional cross section view). The intricate profile with the presence of multi cells both in radius and latitude is clearly visible. Clockwise circulations are shown as solid contours. Typical velocity are about 25 ms^{-1}.

In Figure 6 we display the meridional circulation realized in case *M3*. This meridional circulation is maintained by buoyancy forces, Reynolds stresses, pressure gradients, Maxwell stresses, and Coriolis forces acting on the differential rotation (see Gilman & Miesch 2004). Since these relatively large forces nearly cancel one another, the circulation can be thought as a small departure from (magneto)-geostrophic balance, and the presence of a magnetic field can clearly influence its subtle maintenance. In case *M3*, the meridional circulation exhibits a multi-cell structure both in latitude and radius, and possesses some asymmetry with respect to the equator. Over the temporal period sampled, two vertical cells are present at low latitudes in the northern hemisphere whereas only one, with a rather irregular shape, is present in the southern hemisphere. Other temporal samplings reveal different profiles but in the large they all possess multi-cell structures. Since the convection possesses some asymmetry (cf. Fig. 2) it is not surprising that the meridional circulation does the same.

Given the competing processes for its origin, this weak flow is not straightforward to predict. Typical amplitudes for the velocity are of order 25 m s^{-1}, comparable to local helioseismic deductions (Haber et al. 2002). The flow near the outer boundary is directed poleward at low latitudes, with return flow deeper down. The temporal fluctuations in the meridional circulation are large and thus stable time averages are only attained by frequent sampling over many rotation periods. The kinetic energy contained in the meridional circulation (MCE) (see Fig. 1) is about two orders of magnitude smaller than that contained in the differential rotation and convective motions and is more than an order of magnitude less than the total magnetic energy (ME). As a result, small fluctuations in the convective motions, differential rotation and Lorentz forces can lead to major variations in the circulation.

The shape of the meridional circulation is an important ingredient of solar dynamo models of the flux transport type. These models are built with one large-scale circulation (per hemisphere) and the speed of the flow is used to control the timing of the solar cycle. The presence of a second meridional cell in latitude, as revealed by local helioseismology (Haber et al. 2002), does not seem as problematic for this type of the solar dynamo model as two meridional cells in radius would be (Dikpati these proceedings). It is worth recalling that our simulations generally possess at least two cells as a function of depth with return flows rather deep in the convection zone, thus unattainable by current observational technics to be constrained. It would be interesting to see by how much in these models the timing and the resulting sunspots propagation would be modified by a multi-cells meridional circulation. Precise inversion of the meridional circulation are certainly one of the major challenges of local helioseismology in the year to come. It plays the same pivotal role in today's mean field solar dynamo models that Ω, the differential rotation, played in early 80's. Let's hope that we will be as successful in inverting the meridional circulation as we have been with Ω.

4. THE SOLAR TACHOCLINE

The solar tachocline is the thin region ($< 0.05R$) of strong shear at the base of the solar convection zone ($r \sim 0.713R$), where the differential rotation of the convective envelope changes to solid body rotation in the radiative interior (Corbard et al. 1999). The tachocline plays a crucial role in the solar dynamo since it is most likely the layer where the mean toroidal magnetic field, thought to be at the origin of the surface sunspots, is streched, amplified (by at least a factor of 100 which is not straightforward) and stored until it becomes magnetically buoyant (Parker 1993, Caligari et al. 1998, Fisher et al. 2000, Rempel 2003).

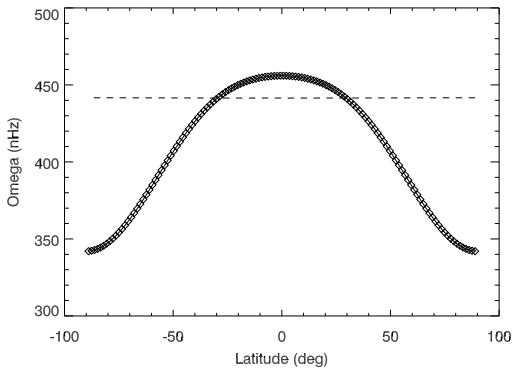

Figure 7. Imposed differential rotation $\Omega_{bcz}/2\pi = 456 - 42\cos^2\theta - 72\cos^4\theta$ *(with* θ *the colatitude) at the top of the stable radiative zone. The dashed line represents* Ω_0*, the rotation rate of the inner shell and of the radiative interior at the start of the simulation.*

However little is known about the dynamics of the solar tachocline: is it turbulent or laminar, what type of circulations are present, what is the dynamical influence of the magnetic fields, why is it so thin extending at most over 5% of the solar radius? Spiegel & Zahn (1992) were the first to address directly some of those questions but in the purely hydrodynamical context. They showed that if no processes where present to oppose its radiative spread, the solar tachocline would extend over 30% of the solar radius after 4.6 Gyr, in complete contradiction with current helioseismic inversions (Corbard et al. 1999). By taking into consideration in their theoretical model anisotropic turbulence (due to the pummeling of the turbulent convective plumes on the top of the stratified radiative interior), they demonstrate

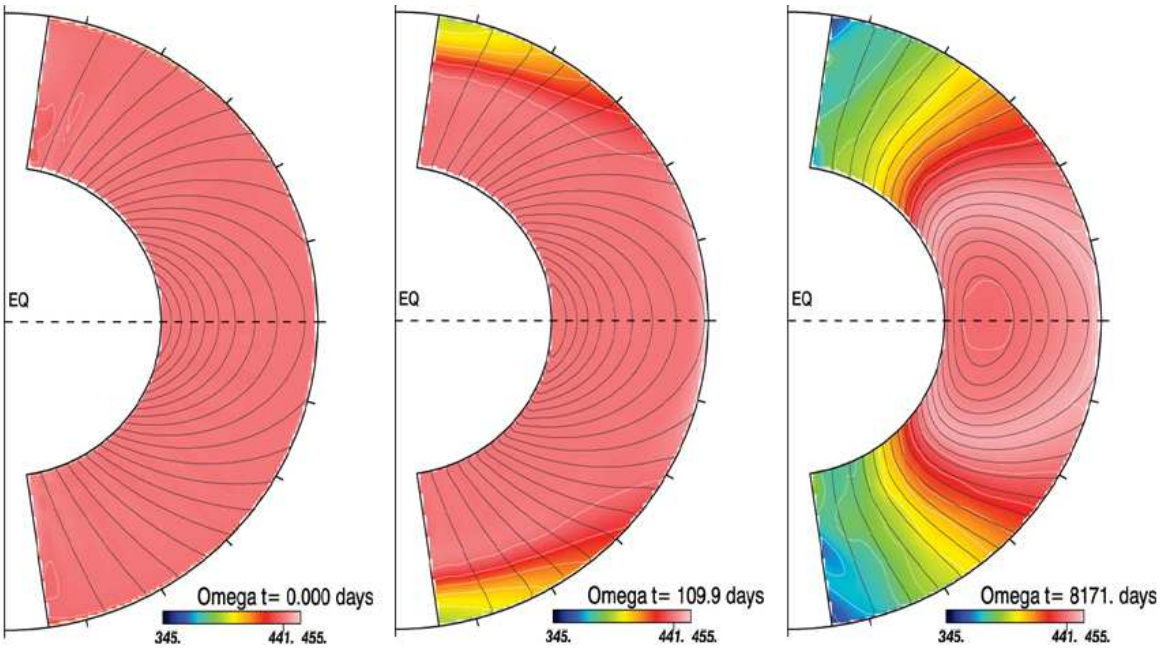

Figure 8. Temporal sequence of the angular velocity (color contours) and of the poloidal magnetic field (black lines) for case T1 over a period equivalent in the model to 10 thermal diffusion time.

that this process could hinder the spread of the solar tachocline to only few % of the solar radius. Their model thus support a turbulent tachocline that does not require the presence of magnetic fields to remain thin but do not exclude it either. Elliott (1997) confirmed their results numerically with a 2–D axisymmetric hydrodynamic code using finite differences. Miesch (2003) using a thin layer version of the ASH code, showed that the coupling between randomly forced turbulence and an imposed shear flow gives rise to Reynolds stresses that transport angular momentum such as to reduce the shear, adding weight to Spiegel & Zahn's model.

Several authors (Rudiger & Kitchatinov 1997; Gough & Mc Intyre 1998; MacGregor & Charbonneau 1999; Garaud 2002) have proposed that the magnetic torques exerted by a weak fossil magnetic field could oppose the inward thermal hyperdiffusion (or viscous diffusion when thermal effect are neglected) of the solar tachocline. Such models favor a slow, rather laminar version of the tachocline. Gilman and collaborators (Gilman these proceedings; Dikpati, Cally & Gilman 2004 and references therein) developped a series of models that showed that the tachocline could become unstable through magnetic instability of toroidal structures embedded within it, resulting in a latitudinal angular momentum transport that suppress the shear and limit its inward diffusion. Forgacs-Dajka (2004) considered the effect of an oscillating dynamo field and found that it could too suppress the spread of the solar tachocline. This increasing number of models of the solar tachocline demonstrates how important characterizing its dynamical properties is. We believe that the ASH code could positively contribute to these ongoing efforts to model the solar tachocline. We thus present here prelimanary results that intend to address the possibility for a dipolar field to stop the spread of the tachocline deeper in the radiative interior in full 3–D simulations for the first time.

4.1. Model Description

We use the ASH code to model the solar radiative interior from $r = 0.3$ to $r = 0.71R$. We assume a stable stratification throughout the computational domain deduced from the 1–D solar model used in our turbulent simulations of the solar convection zone (cf. §3 and Brun et al. 2002). The resolution used is $N_r \times N_\theta \times N_\phi = 128 \times 256 \times 512$. As boundary conditions we assume a constant radiative flux and impenetrable wall and match to a potential field at the top and bottom of the domain and stress free velocity condition at the bottom. At the top of the computational domain we imposed a latitudinal shear of the form $\Omega_{bcz}(\theta)/2\pi = A + B\cos^2\theta + C\cos^4\theta$, with $A = 456$, $B = -42$ and $C = -72$ nHz, that fits reasonnably well the solar differential rotation profile (see Fig. 7). Following Gilman et al. (1989), we deduce the angular velocity of the radiative interior Ω_0 that balances torques at the interface of a convection zone rotating like Ω_{bcz}:

$$\Omega_0/2\pi = A + B/5 + 3/35C = 441 \text{ nHz} \qquad (1)$$

It is interesting to note that helioseismic inversions of

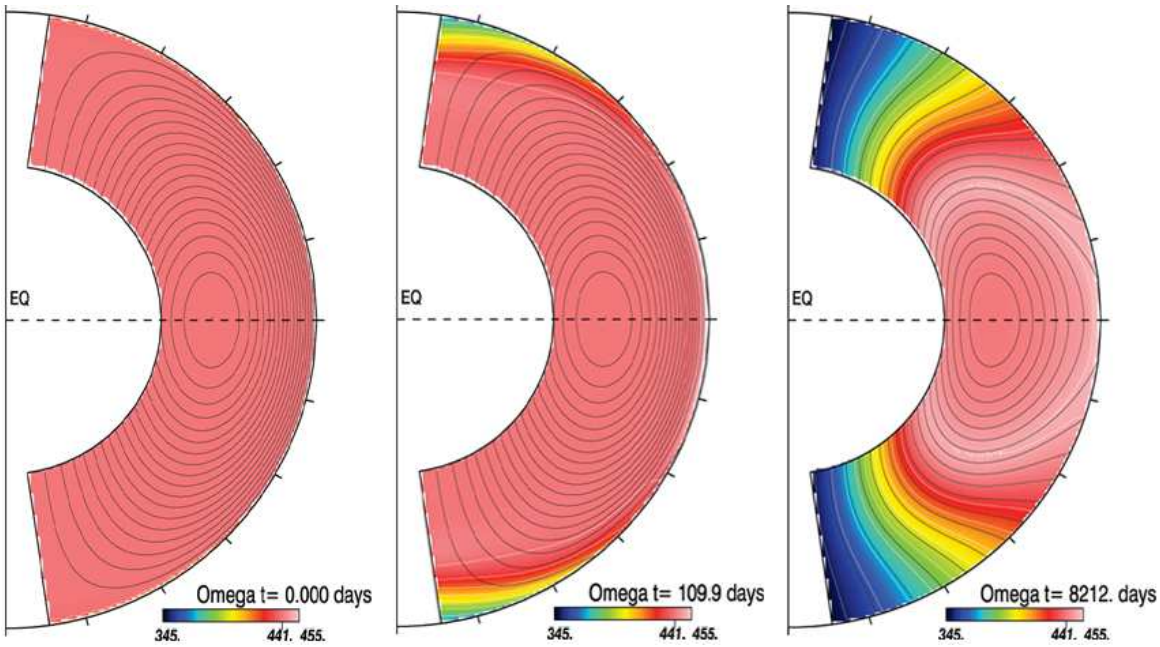

Figure 9. Time evolution of the angular velocity (color contours) and of the poloidal magnetic field for case T2 (started with a confined dipolar magnetic field), over a period equivalent in the model to 10 thermal diffusion time.

the rotation of the radiative interior (down to $0.2R$, Couvidat et al. 2003, Thompson et al. 2003) infer an almost flat profile (solid body rotation) that rotates to value very close to Ω_0. This means that even in the real Sun, the exchange through the interface between the convection and the radiation zone are nearly balanced, with only a weak torque operating there. How the angular momentum lost through the solar wind and resulting in the spin down of the Sun influence the redistribution of angular momentum in the radiative interior and in the tachocline is definitely not an easy question to answer (see Gilman et al. 1989). The fact that the torques are almost balanced at the base of the solar convection indicate that the outward transfer of angular momentum from the deep interior to the convective envelope must occur on a slow time scale.

In cases T1 and T2 presented here we use Prandtl, magnetic Prandtl and Roberts numbers $Q = \eta/\kappa$ of respectively 1/100, 1 and 1/100. These two cases differ by their initial dipolar field which is either open, going through the top boundary or confined below it (as in configurations $D1$ and $D3$ of MacGregor & Charbonneau 1999). Our choice of parameters and Prandtl number ($Pr < 0.01$) for cases T1 & T2 means that thermal hyperdiffusion dominates over viscous diffusion (see eq. 4.10 of Spiegel & Zahn 1992) and that the relevant time scales are the Ohmic and thermal ones.

4.2. Results

Figures 8 and 9 display the temporal evolution of the angular velocity Ω of cases T1 and T2, with the poloidal fields superimposed. The left panels of Figures 8 and 9 represent both the initial solid body rotation state of the radiative zone and the dipolar field (either open or confined) used to start the temporal evolution. We see in the middle panels of these Figures that the imposed shear starts to propage in the radiative interior at rather high latitudes. The rate of propagation seems faster in case T1 than it is in case T2. In T1, the field lines are too radial at those high latitudes to oppose the inward diffusion. On the contrary in case T2 the field lines are much more horizontal and can exert a force that slows down a bit the thermal hyperdiffusion. The strength of the dipole field is slowly decaying away since no processes can yet regenerate it. After over 10 thermal diffusion time scale, the angular velocity profile in the radiative interior does not look at all as it started (right panels of Fig. 8 & 9). Wherever the field lines cross the top boundary, the imposed shear has propagated all the way down to the bottom of the domain. In case T1, Ferraro's law of isorotation at high latitude is not exactly satisfied, and the shear stretches the poloidal field lines, inducing the generation of a rather strong mean toroidal magnetic field. Such generation is, at our surprise, maintained over many Ohmic diffusion time scales but does not yet trigger an instability that could regenerate the poloidal field. In case T2, the toroidal field first grows and then decays away. At mid latitude a ring of prograde

rotation surrounds the last zone in the shell possessing uniform rotation. As the time evolves and more magnetic field lines diffuse through the top boundary, the fast rotating rings shrink in size and the imposed shear gets to lower latitudes. Our simulations also revealed the presence of a weak single cell meridional circulation per hemisphere in the tachocline, directed poleward at the top of the domain.

Our simulations show that a fossil dipole field is not that efficient at limiting the inward thermal hyperdiffusion of a latitudinal shear, once its fields lines have connected with the region where the shear is imposed. Whether in the real Sun, the fossil dipolar field lines connect or not with the convection zone is another challenging question to be answered and could modify the conclusion of our study. We intend to attack this problem in the near future.

However our model can help answering other questions. For instance, since our model of the solar tachocline is fully 3–D, $m = 1$ or $m = 2$ instabilities of the toroidal field, as Dikpati et al. (2004) suggest should appear over a certain threshold amplitude for B_ϕ, could develop in the strong shearing region near the top of the domain. Unfortunately, we have not yet found in our simulations, even in case T1, that the toroidal fields amplified in the evolving tachocline through ω-effect become unstable. We are guessing that the toroidal field strength attained in our simplified model of the solar tachocline are not large enough (10 kG instead of 100 kG) to trigger the instability. As we scan the space parameters we will keep looking for the instability of B_ϕ, since we will be able to study its nonlinear evolution and it could potentially provide a way to regenerate the mean poloidal field.

5. PERSPECTIVES

We have shown that numerical simulations of the complex solar magnetoydrodynamics are becoming more and more tractable with today's supercomputers. In particular we have studied how turbulent convection under the influence of rotation can establish a strong differential rotation and weak meridional circulation, generate magnetic fields through dynamo action and how Lorentz forces act to diminish the differential rotation by having Maxwell stresses transporting angular momentum poleward and thus opposing the Reynolds stresses. Many challenges remain, among them the understanding of the two shear layers present at the base (the tachocline) and at the top of the solar convection zone is a priority since these layers are directly linked to the solar dynamo (Ossendrijver 2003) and subsurface weather (Haber et al. 2002). Another challenge is to get a more accurate and deeper inversion of the meridional circulation present in the solar convection since it plays a crucial role in current mean field solar dynamo models (Dikpati these proceedings). Our numerical simulations favor a multi-cells structure for the meridional circulation whereas flux transport models assume one large cell. This issue need to be clarified. In order to progress in our understanding of the solar interior, we have started to study with ASH in three dimensions under the MHD anelastic approximation, the solar tachocline and radiative zone. We have considered how a dipolar magnetic field could oppose the radiative spread of the tachocline. We have found that the magnetic field have a tendency to diffuse outward through the shell and to communicate to the radiative interior, first, at high, then at lower latitudes, the imposed latitudinal shear at the top of the domain, therefore enforcing an isorotation of Ω along the poloidal field lines. This behavior is known as Ferraro's law of isorotation. As a result only a small region near the equator rotates uniformly. We further considered confined or open magnetic field configurations as in MacGregor & Charbonneau (1999), but did not find significative differences, except that the latter amplifies and sustains more efficiently a mean toroidal field. Work is in progress to compute with ASH in one single global model the solar convection and radiation zones (using two stacked Chebyshev domains). These simulations will provide a first step toward a self-consistent, high resolution model of the solar dynamo. Another improvement could be to incorporate in our simulations of turbulent convection a more realistic equation of state and detailed description of the radiative transfer of the solar near surface shear layer along with a more accurate subgrid scale (SGS) model. As a final remark, we would like to note that a promising numerical methods is emmerging, the spectral-element method (Karniadakis & Sherwin 1998), that combines the exponential accuracy convergence of the pseudo-spectral methods with the flexibility of the finite elements methods. A new 3–D MHD code making use of this powerful approach would certainly result in a significant step forward in solar modelling.

ACKNOWLEDGEMENTS

The author is grateful to J. Leibacher, M.S. Miesch, J. Toomre, S. Turck-Chièze & J.-P. Zahn for their support and the many years of fruitful discussions. They author would also like to thank the organizers of the SoHO14-GONG04 meeting for their invitation, especially S. Basu. The simulations with ASH were carried out with NSF NPACI support to various american supercomputer centers and with CEA and CNRS support to various french supercomputer centers.

REFERENCES

- Biskamp, D. 1993, Nonlinear Magnetohydrodynamics (Cambridge: Cambridge Univ. Press)
- Brandenburg, A., Jennings, R. L., Nordlund, Å., Rieutord, M., Stein, R. F., Tuominen, I. 1996, JFM, 306, 325
- Brummell, N. H., Hurlburt, N. E., & Toomre, J. 1998, ApJ, 493, 955
- Brun, A. S. 2004, Solar Phys., 220, 333
- Brun, A. S., & Toomre, J. 2002, ApJ, 570, 865
- Brun, A. S., Antia, H. M., Chitre, S. M. & Zahn, J.-P. 2002, A&A, 391, 725
- Brun, A. S., Miesch, M. S. & Toomre, J. 2004, ApJ, 614, in press
- Brun, A. S., Miesch, M. S. & Toomre, J. 2005, in preparation
- Caligari, P., Schuessler, M. & Moreno-Insertis, F. 1998, 502, 481
- Cattaneo, F. & Hughes, D. W. 2001, Astron. & Geophys., 42, 3, 18
- Clune, T. L., Elliott, J. R., Glatzmaier, G. A., Miesch, M. S., & Toomre, J. 1999, Parallel Comput., 25, 361
- Corbard, T., Blanc-Féraud, L., Berthomieu, G. & Provost, J. 1999, A&A, 344, 696
- Couvidat, S., Garcia, R. A., Turck-Chi'eze, S., Corbard, T., Heney, C. J. & Jiménez-Reyes, S. 2003, 597, L77
- DeRosa, M. L., Gilman, P. A. & Toomre, J. 2002, ApJ, 581, 1356
- Dikpati, M. & Charbonneau, P. 1999, ApJ, 518, 508
- Dikpati, M., Cally, P. S. & Gilman, P. A., 2004, ApJ, 610, 597
- Dikpati, M. these proceedings
- Durney, B. R. 1999, ApJ, 511, 945
- Eddy, J. A., Gilman, P. A. & Trotter, D. E. 1976, Solar Phys., 46, 3
- Elliott, J. 1997, A&A, 327, 1222
- Fisher, G. H., Fan Y., Longcope, D. W., Linton, M. G. & Pevtsov, A. A. 2000, Solar Phys., 192, 119
- Forgacs-Dajka, E. 2004, A&A, 414, 1143
- Garaud, P. 2002, MNRAS, 329, 1
- Gilman, P. A. 1983, ApJS, 53, 243
- Gilman, P. A., Morrow, C. A. & DeLuca, E. E. 1989, ApJ, 338, 528
- Gilman, P. A., Dikpati, M. & Miesch, M. S. these proceedings
- Gilman, P. A. & Miesch, M. S., 2004, ApJ, 611, 568
- Glatzmaier, G. A. 1987, in The Internal Solar Angular Velocity, ed. B. R. Durney & S. Sofia (Dordrecht: D. Reidel), 263
- Glatzmaier, G. A., & Gilman, P. 1982, ApJ, 256, 316
- Gough, D. O. & McIntyre, M. E. 1998, Nature, 394, 755
- Haber, D. A., Hindman, B. W., Toomre, J., Bogart, R. S., Larsen, R. M., & Hill, F. 2002, ApJ, 570, 855
- Karniadakis, G. E., & Sherwin, S. J. 1998, Spectral/hp Element Methods for Cfd (Oxford: Oxford Univ. Press)
- Kichatinov, L. L., & Rüdiger, G. 1995, A&A, 299, 446
- MacGregor, K. B. & Charbonneau , P. 1999, ApJ, 519, 911
- Miesch, M. S., Elliott, J. R., Toomre, J., Clune, T. L., Glatzmaier, G. A., & Gilman, P. A., 2000, ApJ, 532, 593
- Miesch, M. S. 2003, ApJ, 586, 663
- Ossendrijver, M. 2003, Astron. Astrophys. Rev., 11, 287
- Pedlosky, J., 1987, Geophysical Fluid Dynamics (New York: Springer)
- Parker, E. N. 1993, ApJ, 408, 707
- Rempel, M. 2003, A&A, 397, 1097
- Robinson, F. J., these proceedings
- Robinson, F. J. & Chan, K. L. 2001, MNRAS, 321, 723
- Rudiger & Kitchatinov 1997, Astron. Nach., 318, 273
- Spiegel, E. A. & Zahn, J.-P. 1992, A&A, 265, 106
- Stein, R. F. & Nordlund Å. 2000, Solar Phys., 192, 91
- Stix, M. 2002, The Sun: an introduction, 2nd ed, (Berlin: Springer-Verlag)
- Thompson, M. J., Christensen-Dalsgaard, J., Miesch, M. S. & Toomre, J. 2003, Ann. Rev. Astron. Astrophys., 41, 599
- Tobias, S. M., Brummell, N. H., Clune, T.L. & Toomre, J. 2001, ApJ, 549, 1183
- Weiss, N. O. 1994, in Lectures on Solar and Planetary Dynamos, ed. M. R. E. Proctor & A. D. Gilbert (Cambridge: Cambridge Univ. Press), 59